Journal of Materials Chemistry

Cite this: J. Mater. Chem., 2012, 22, 520

www.rsc.org/materials

PAPER

Nonvolatile bistable resistive switching in a new polyimide bearing 9-phenyl-9*H*-carbazole pendant†

Benlin Hu,[ab] Fei Zhuge,*[ab] Xiaojian Zhu,[ab] Shanshan Peng,[ab] Xinxin Chen,[ab] Liang Pan,[ab] Qing Yan[ab] and Run-Wei Li*[ab]

Received 9th August 2011, Accepted 23rd September 2011
DOI: 10.1039/c1jm13849a

A new polyimide bearing the functional pendant 9-phenyl-9*H*-carbazole moieties, poly[2,2-(4,4′-di(*N*-benzyloxycarbazole)-3,3′-biphenylene)propane-hexafluoroisopropylidenediphthalimide] (6F-BAHP-PC PI), has been designed as a functional material for resistance memory devices. The ITO/6F-BAHP-PC PI/Ag memory device exhibits nonvolatile resistive switching (RS) with a high ON/OFF ratio (>10^6), long retention time (>6×10^4 s), good endurance, and low power consumption (~100 μW). *In situ* conductive atomic force microscopy measurements show that the RS of 6F-BAHP-PC PI originates from the formation/rupture of nanoscale conducting filaments.

Introduction

Over the past decade, resistance random access memory (RRAM) based on resistive switching (RS) has attracted much attention as a next generation nonvolatile memory due to its excellent properties, for instance, simple structure, mass storage, high operation speed, and compatibility with traditional CMOS technology. Since the RS phenomenon was first discovered in the $Al/Al_2O_3/Al$ sandwiched structure in 1962,[1] a large number of inorganic materials have been reported to show RS, such as chalcogenides,[2] complex oxides,[3–5] binary oxides,[6–8] and amorphous carbon.[9] Recently, some polymer systems have also been found to exhibit RS effect, including conjugated polymers,[10–15] functional polyimides (PIs),[16–28] polymers with specific pendent chromophores,[29–32] and polymer nanocomposites (embedded with metal nanoparticles,[33–36] fullerene,[30] carbon nanotubes,[37–39] or graphene oxide[40–42]). Compared to chalcogenides and oxides which have been investigated quite extensively as RS materials, polymeric materials are more attractive for RRAM applications due to significant advantages, such as high scalability and highly tailorable properties. And also, polymeric materials possess the advantages of rich structure modifications, easy solution processability, flexibility, low-cost, high mechanical strength and three-dimensional stacking capability.[11,43–46]

PI containing both electron donor and acceptor moieties within a repeating unit has been found to exhibit bistable RS attributed to an electronic transition process between the ground and excited states, which could be achieved by the induced charge transfer from donor to acceptor under applied electric fields.[16–28] However, the endurance behavior of the PI-based RRAM devices has rarely been explored. Furthermore, no direct experimental evidence has been given for the RS mechanism of PIs. On the other hand, carbazole is a well-known hole-transporting unit and electron donor unit. Carbazole derivatives exhibit high charge mobility and a large band gap attributed to the improved planar biphenyl unit by the bridging nitrogen atom.[47] Polymers with carbazole unit in the main chain or as a pendant group have been widely investigated due to their unique properties for many potential applications, such as photoconduction,[48] electroluminescence,[48–50] memory[17,29,44,51,52] and photorefraction[53] materials. Ree and co-workers[17] reported a PI functionalized with 9*H*-carbazole-9-ethanol, showing RS behavior. However, the conjugate region of the functional pendant 9*H*-carbazole-9-ethanol is not large enough and consequently can not support a stable highest occupied molecular orbital (HOMO) energy.

Herein, we report a PI bearing 9-phenyl-9*H*-carbazole pendant, a better hole-transporting unit with larger conjugated confines and better oxidative stability compared to 9*H*-carbazole-9-ethanol,[17] poly[2,2-(4,4′-di(*N*-benzyloxycarbazole)-3,3′-biphenylene)propane-hexafluoroisopropylidenediphthalimide] (6F-BAHP-PC PI), which shows excellent nonvolatile RS characteristics. This PI is soluble in common organic solvents so that the PI thin films can be easily prepared by a conventional spin-coating method. The RRAM devices with this PI as storage medium exhibit good memory characteristics, including high ON/OFF ratios, low operation voltages, low power consumption, long retention times, and good endurance. Conductive atomic force microscopy (C-AFM) measurements show that the

[a]*Key Laboratory of Magnetic Materials and Devices, Ningbo Institute of Material Technology and Engineering, Chinese Academy of Sciences, Ningbo, 315201, China. E-mail: zhugefei@nimte.ac.cn; runweili@nimte.ac.cn*
[b]*Zhejiang Province Key Laboratory of Magnetic Materials and Application Technology, Ningbo Institute of Material Technology and Engineering, Chinese Academy of Sciences, Ningbo, 315201, China*
† Electronic supplementary information (ESI) available. See DOI: 10.1039/c1jm13849a

RS of 6F-BAHP-PC PI originates from the formation/rupture of nanoscale conducting filaments. This study suggests that 6F-BAHP-PC PI is a promising material for RRAM applications.

Experimental

Materials

Carbazole, 4-fluorobenzaldehyde, potassium *tert*-butoxide and 2,2-bis(4- hydroxyphenyl)propane were obtained from Aladdin reagent Co. and used as received. 4,4′-(Hexafluoroisopropylidene)diphthalic anhydride (6FDA) was obtained from Changzhou Sunlight Pharmaceutical Co., Ltd. and sublimated before use. 2,2-Bis(3-amino-4-hydroxyphenyl)propane (BAHP) was synthesized and purified according to the method reported in ref. 54. All the other reagents and solvents were analytical grade and without further purification.

Instrumentation

The ^{1}H nuclear magnetic resonance (^{1}H NMR) spectra were measured at 400 MHz on a Bruker 400 AVANCE III spectrometer, using dimethyl sulfoxide-d_6 (DMSO-d_6) or *N*,*N*-dimethylformamide-d_7 (DMF-d_7) as solvent. The Fourier transform infrared (FT-IR) spectra were obtained with a Thermo Nicolet 6700 FTIR spectrometer, where the polymer samples were films with thickness ~2 μm. The UV-vis absorption spectra were recorded on a Perkin Elmer lambda 950 spectrophotometer at room temperature. The inherent viscosities were measured with an Ubbelodhe viscometer at 30 ± 0.1 °C in *N*-methyl-2-pyrrolidone (NMP) at a concentration of 0.5 g dL^{-1}. Thermogravimetric analysis (TGA) was performed on a Perkin-Elmer Diamond TG/DTA instrument at a heating rate of 10 °C min^{-1} under nitrogen atmosphere with a flow rate of 50 mL min^{-1}. Differential scanning calorimetry (DSC) measurements were carried out with Mettler Toledo DSC at a heating rate of 10 °C min^{-1} under a nitrogen atmosphere with 50 mL min^{-1} gas flow, where the glass transition temperature was reported as temperature in the middle of the thermal transition from the second heating scan. Gel permeation chromatography traces of the samples were recorded on a Viscotek T60A/LR40 GPC system, where chloroform was used as the eluent, and linear polystyrene was used as the standard. Cyclic voltammetry (CV) measurements were carried out in a 0.1 M solution of tetrabutylammonium hexafluorophosphate (n-Bu$_4$NPF$_6$) in acetonitrile under an argon atmosphere with a platinum gauze as counter electrode and an Ag/AgCl (3.8 M KCl) reference electrode. A scan rate of 100 mV s^{-1} was used during the CV measurements. Atomic force microscopy (AFM) characterization was conducted by a Veeco Dimension 3100 V scanning probe microscope in ambient conditions using a tapping or CAFM mode.

Synthesis of monomers and polyimides

Synthesis of 4-carbazol-9-ylbenzaldehyde (1 in Scheme 1). Carbazole (8.40 g, 0.05 mol) and potassium *tert*-butoxide (5.61 g, 0.05 mol) were mixed in 200 mL anhydrous *N*,*N*-dimethylformamide (DMF) and heated to 110 °C, and then 4-fluorobenzaldehyde (6.20 g, 0.05 mol) dissolved in DMF was dropped into the mixture over 50 min. The mixture was maintained at 110 °C for about 36 h. Then the mixture was cooled to room temperature, and poured into 700 mL ice water. The precipitate was filtered and dried. The pale yellow compound was crystallized from acetone/water (v/v = 10 : 1), yield 60%. ^{1}H NMR (DMSO-d_6, δ, ppm): 10.12 (s, 1H), 8.26 (d, 2H, J = 8.0 Hz), 8.19 (d, 2H, J = 8.4 Hz), 7.90 (d, 2H, J = 8.4 Hz), 7.52 (d, 2H, J = 8.0 Hz), 7.46 (t, 2H, J = 7.6 Hz), 7.33 (t, 2H, J = 7.2 Hz); IR (KBr): 3418 (s), 3050 (w), 1595(s), 1510 (m), 1482 (w), 1445 (s), 1360 (m), 1337 (m), 1221 (m), 1157 (m), 1125 (m), 832 (m), 753 (s).

Synthesis of (4-(9*H*-carbazol-9-yl)phenyl)methanol (CPM, 2 in Scheme 1). A solution of sodium borohydride (0.196 g, 5.2 mmol) in 1 M aqueous NaOH (10.5 mL) was added dropwise to a suspension of 4-carbazol-9-ylbenzaldehyde (2.71 g, 10 mmol) in ethanol (35 mL) under nitrogen. After stirring for 4 h, most of the insoluble starting material was reacted. The reaction mixture was poured into dichloromethane (42 mL) and washed with water (3 × 40 mL). The organic layer was dried over magnesium sulfate and most of the solvent removed under reduced pressure. The pure product CPM was obtained by crystallization from dichloromethane/n-hexane (*v*/*v* = 1 : 1), yield 74%. ^{1}H NMR (DMSO-d_6, δ, ppm): 8.24 (d, 2H, J = 7.6 Hz), 7.61 (d, 2H, J = 8.4 Hz), 7.56 (d, 2H, J = 8.4 Hz), 7.42 (t, 2H, J = 7.4 Hz), 7.35 (d, 2H, J = 8.4 Hz), 7.28 (t, 2H, J = 7.2 Hz), 5.37 (t, 1H, J = 5.6 Hz), 4.65 (d, 2H, J = 5.6 Hz); IR (KBr): 3200 ~ 3600 (br), 1607 (w), 1595 (w), 1517 (m), 1477 (m), 1450 (s), 1226 (m), 750 (s), 726 (s).

Synthesis of 6F-BAHP PI (Scheme 2). 6FDA (0.8887 g, 2 mmol) and BAHP (0.5167 g, 2 mmol) were dissolved together in dry NMP (6 mL) with isoquinoline (0.45 mL) as a catalyst. The reaction mixture was gently heated to 70 °C under stirring for 2 h, followed by refluxing for 5 h. The reaction solution was diluted with 18 mL NMP and then poured into a mixture of 100 mL methanol and 100 mL water under vigorous stirring. The precipitate was filtered, washed with hot methanol and dried in vacuum, giving the target PI product. ^{1}H NMR (DMF-d_7, δ, ppm): 10.14 (s, 2H, Ar–OH), 8.21 (d, 2H, Ar–H), 8.08 (d, 2H, Ar–H), 7.95 (d, 2H, Ar–H), 7.47 (d, 2H, Ar–H), 7.20 (d, 2H, Ar–H), 7.02 (d, 2H, Ar–H), 3.51 (s, 6H, CH$_3$). IR (film): 3200 ~ 3600 (br), 1785 (m), 1721 (s), 1618 (m), 1513 (s), 1432(m), 1383 (s), 1256 (s), 1110 (m), 722 (m).

Synthesis of 6F-BAHP-PC PI (Scheme 2). The obtained 6F-BAHP PI further reacted with the CPM. 6F-BAHP PI (0.6690 g, 1.0 mmol), CPM (1.0933 g, 4 mmol) and triphenyl phosphine (1.0492 g, 4 mmol) were dissolved in dry tetrahydrofuran (THF) (10 mL) under nitrogen atmosphere. Diisopropyl diazocarboxylate (0.8088 g, 4 mmol) in dry THF (2.5 mL) was then added dropwise into the reaction mixture. The reaction mixture was stirred at room temperature for 24 h. Then

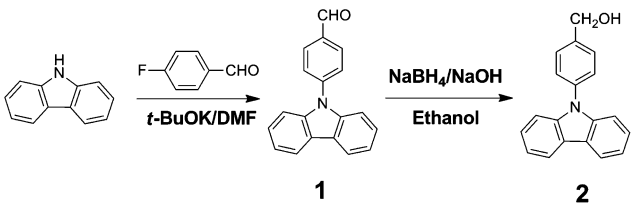

Scheme 1 Synthesis of CPM monomer.

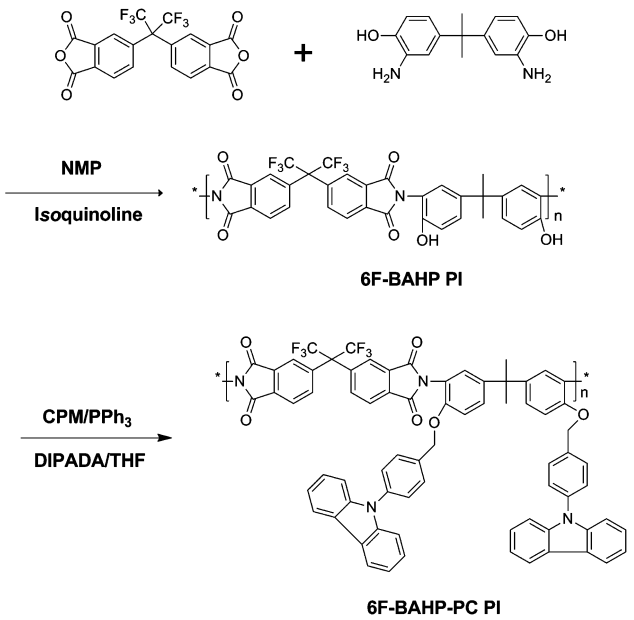

Scheme 2 Synthesis of 6F-BAHP PI and 6F-BAHP-PC PI polymers.

the reaction solution was diluted with 21 mL THF and poured into 220 mL methanol under vigorous stirring, giving the target polymer product as precipitate. The precipitate was filtered, washed with hot methanol, and dried in vacuum. The obtained polymer was identified as poly[2,2-(4,4′-di(*N*-benzyloxycarbazole)-3,3′-biphenylene)propane-hexafluoroiso propylidenediphthalimide] (6F-BAHP-PC PI) by ^{1}H NMR spectroscopy. ^{1}H NMR (DMF-d_7, δ, ppm): 8.23–7.23 (m, 36H), 5.34 (s, 4H, CH_2), 3.50 (s, 6H, CH_3); IR (film): 1786 (m), 1728 (s), 1610 (w), 1598 (w), 1517 (s), 1452(m), 1373 (s), 1257 (m), 1110 (m), 750 (m), 723 (m).

Fabrication and characterization of the memory device

The ITO coated glass substrates were pre-cleaned sequentially with ethanol, acetone and isopropanol in an ultrasonic bath for 20 min, respectively. A 0.2 mL cyclopentanone solution of the 6F-BAHP-PC PI (1.0 wt % polymer) was spin-coated onto the ITO substrates at a spinning rate of 400 rpm for 12 s and 2000 rpm for 40 s, followed by drying in vacuum at 80 °C for 8 h. Before spin-coating, the solution was filtered through polytetrafluoroethylene (PTFE) membrane micro-filters with a pore size of 0.45 μm. The PI film thickness was about 80 nm, measured using a spectroscopic ellipsometer (model M2000DI, Woollam). In order to measure the electrical properties, Ag top electrodes of about 150 nm in thickness were deposited at room temperature by magnetron sputtering system with an *in situ* metal shadow mask. The current–voltage (*I–V*) characteristics of ITO/6F-BAHP-PC PI/Ag structures were measured in ambient atmosphere using a Keithley 4200 semiconductor characterization system with a voltage sweeping mode. The sweeping step is 0.01 V. During the measurement, a bias voltage was applied between the top (Ag) and bottom (ITO) electrodes with the latter being grounded.

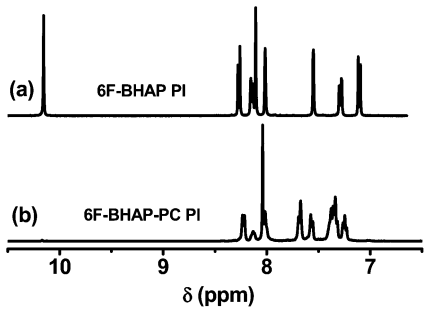

Fig. 1 ^{1}H NMR spectra of (a) 6F-BAHP PI and (b) 6F-BAHP-PC PI.

Results and discussion

Characterization of polymer structures

A new functional compound bearing 9-phenyl-9*H*-carbazole moieties, CPM, was synthesized with a yield of 74% (Scheme 1). As shown in Scheme 2, 6F-BAHP-PC PI was synthesized in a two-step method. Firstly, soluble 6F-BAHP PI was synthesized directly from the polycondensation of the respective monomers using isoquinoline as a catalyst. Fig. 1(a) shows the ^{1}H NMR spectrum of as-grown 6F-BAHP PI (the original NMR spectrum of 6F-BAHP PI is described in Fig. S1 in the ESI†). The proton peak of the hydroxyl side groups can be observed at 10.14 ppm, and the characteristic peaks of the aromatic rings at 7.02–8.21 ppm and the proton peak of the isopropyl groups at 3.51 ppm are also observed. No characteristic peaks of amino protons are detected in the ^{1}H NMR suggesting that the product contains a negligible amount of partially imidized 6F-BAHP poly(amic acid). It proves that the 6F-BAHP PI has been successfully synthesized. Secondly, 6F-BAHP-PC PI was obtained by incorporating CPM moieties into the soluble 6F-BAHP PI. As shown in Fig. 1(b), the ^{1}H NMR spectrum of 6F-BAHP-PC PI does not show any hydroxyl peak originating from the 6F-BAHP PI (the original NMR spectrum of 6F-BAHP-PC PI is described in Fig. S2 in the ESI†). Fig. 2 shows FT-IR spectra of 6F-BAHP PI and 6F-BAHP-PC PI. The formation of polyimides can be confirmed by the peaks at ~1780 and 1727 cm^{-1}, which are assigned to the vibrating peaks of imide rings. The IR spectrum of 6F-BAHP-PC PI (Fig. 2(b)) shows double peaks at 750 and 723 cm^{-1}, which are the characteristic peaks of *ortho*-position aromatic protons of two phenyl of carbazole moieties. The IR

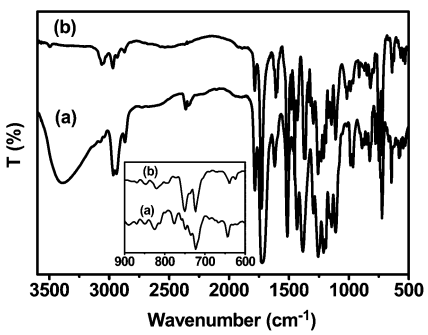

Fig. 2 FT-IR spectra of (a) 6F-BAHP PI and (b) 6F-BAHP-PC PI films. The inset is the enlarged spectra.

spectrum of 6F-BAHP PI (Fig. 2(a)) shows a broad peak in the range 3600–3200 cm^{-1}, while this peak disappears in Fig. 2(b). The above analysis indicates that the hydroxyl groups of the 6F-BAHP PI have been completely replaced by CPM moieties. The 6F-BAHP-PC PI shows an inherent viscosity of 1.54 dL g^{-1} in NMP. The weight-average molecular weight of the 6F-BAHP-PC PI is 568916 and the polydispersity index is 4.9 by GPC analysis. Such polyimide exhibits good solubility in common solvents, such as DMF, THF, chloroform, cyclohexanone. Fig. 5 (a) shows the AFM image of as-grown 6F-BAHP-PC PI films. The polyimide thin films have a relatively flat surface with a surface roughness of about 0.85 nm from AFM analysis. Therefore, high quality 6F-BAHP-PC PI thin films have been prepared by means of a conventional spin-coating method.

Thermal properties

The thermal properties of the new functional polyimides were evaluated by TGA and DSC under nitrogen atmosphere, as shown in Fig. 3. The 6F-BAHP-PC PI is found to have a degradation temperature ($T_{d\ 10\%}$) of 435 °C and a glass transition temperature (T_g) of 245 °C. The results indicate that the 6F-BAHP-PC PI is a thermally stable polymer, which can be used in the microelectronic industry.

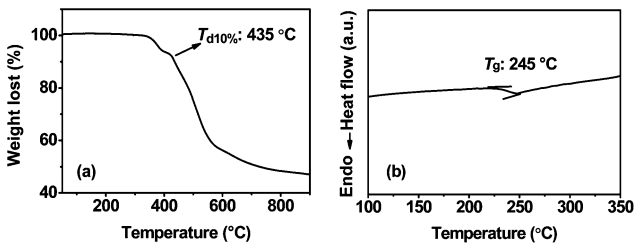

Fig. 3 (a) TGA and (b) DSC curves of 6F-BAHP-PC PI under argon atmosphere at a heating rate of 10 °C min^{-1}.

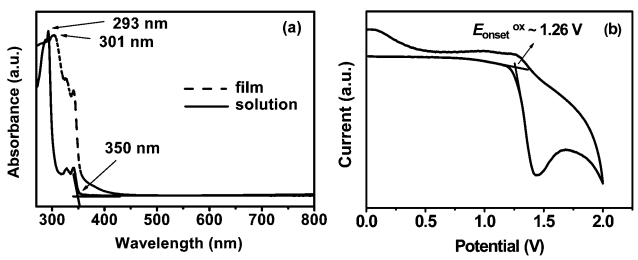

Fig. 4 (a) UV-Vis spectra of 6F-BAHP-PC PI in NMP solution and thin film states. (b) Cyclic voltammograms of 6F-BAHP-PC PI films.

Optical and electrochemical properties

Fig. 4(a) shows the UV-vis absorption spectra of the 6F-BAHP-PC PI in NMP solution and thin film state. The polyimide exhibits absorption peak maxima at around 293 and 301 nm in solution and thin film states, respectively. The absorption peaks are attributed to the π–π* transition delocalized along the π-electronic system. The optical band gap of 6F-BAHP-PC PI is estimated to be 3.54 eV from the onset optical absorbance. Fig. 4 (b) shows the cyclic voltammogram of 6F-BAHP-PC PI thin films with platinum bottom electrodes using a 0.1 M solution of tetrabutylammonium tetrafluoroborate (TBATFB) in anhydrous acetonitrile. The new functional polyimide exhibits reversible *p*-doping behavior during the anodic scan. The onset oxidation potential (E_{onset}^{ox}) of 6F-BAHP-PC PI is around 1.26 V *vs.* Ag/AgCl, which is higher than other triphenylamine (TPA)-based PIs.[20,26] Therefore, the HOMO and lowest unoccupied molecular orbital (LUMO) energy levels of 6F-BAHP-PC PI are −5.74 and −2.20 eV, respectively. These results indicate that the new functional polyimide could provide a lower and more stable HOMO energy level and therefore a charge trapping environment, which may result in more stable RS.

Memory device characteristics of the polymers

The schematic structure of the sandwiched devices is depicted in Fig. 5(b). The memory effects of 6F-BAHP-PC PI films are demonstrated by the *I–V* characteristics of ITO/6F-BAHP-PC PI/Ag memory devices. The polymeric memory devices store data based on the switching between high (OFF) and low (ON) resistance states in response to the external applied voltages. Fig. 5(c) shows a typical *I–V* characteristics of bistable ITO/6F-BAHP-PC PI/Ag memory devices. As can be seen in Fig. 5(c), the as-fabricated device is initially in the OFF state ("0" signal in data storage) with a current in the range of 10^{-12}–10^{-9} A as the voltage sweeps from 0 to about 1.4 V. As the voltage further increases, an abrupt increase in the current occurs in the device around 1.5 V (with a current compliance of 0.1 mA), indicating that the device undergoes a sharp electrical transition from OFF state to ON state ("1" signal in data storage). This OFF-to-ON transition can function in a memory device as a "writing" or "SET" process. The device will remain in the ON state, even after the power is turned off or during sequential forward voltage sweeping with the current compliance maintained at 0.1 mA. By

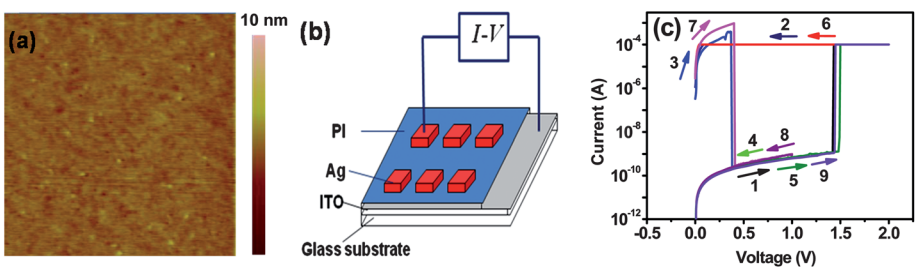

Fig. 5 (a) AFM image of 6F-BAHP-PC PI films with a scanning size of 10 × 10 μm^2. (b) A schematic configuration of the ITO/6F-BAHP-PC PI/Ag devices. (c) *I–V* characteristics of ITO/6F-BAHP-PC PI/Ag memory cells.

applying a positive voltage with a higher current compliance (1 mA), an abrupt decrease in the current occurs in the device at around 0.4 V, indicating that the device is switched from the ON state to OFF state. This ON-to-OFF transition can function in a memory device as an "erasing" or "RESET" process. It is found that an ON/OFF current ratio of the device as high as 10^6 can be achieved, which leads to a low misreading rate for memory applications. The switching power is about 100 μW. The results indicate that ITO/6F-BAHP-PC PI/Ag memory devices exhibit nonvolatile unipolar RS behavior.

In order to investigate the endurance performance of ITO/6F-BAHP-PC PI/Ag memory devices, cyclic switching operations have been conducted. Fig. 6(a) shows the evolution of the resistance of the two well-resolved states over more than 50 cycles. The resistance values were read out at 0.1 V in each voltage sweep. Although there is a slight fluctuation of the resistance in the ON and OFF states, the resistance ratios are more than six orders of magnitude during RS cycles. Fig. 6(b) shows the retention performance of ITO/6F-BAHP-PC PI/Ag devices under 0.1 V durable stress. The measurement was carried out in ambient atmosphere at room temperature using a reading voltage of 0.1 V. As can be seen from Fig. 6(b), the variation of ON and OFF state resistance after 6×10^4 s under 0.1 V durable stress is very little, confirming the nonvolatile nature of the devices.

To understand the conduction and switching mechanisms of ITO/6F-BAHP-PC PI/Ag devices, the *I–V* curves of both SET and RESET processes were replotted in a log-log scale, as shown in Fig. 7. The ohmic conduction model is found to satisfactorily fit the *I–V* curve for the ON state, indicating that ohmic conduction is dominant in the ON state. On the other hand, the conduction mechanisms of the OFF state are much more complicated. Fitting results suggest that the charge transport behavior is in good agreement with a classical trap-controlled space charge limited current (SCLC), which consists of three portions: the ohmic region ($I \propto V$), Child's law region ($I \propto V^2$), and the steep current increase region.[55] Therefore, the dominant conduction mechanism of the OFF state is trap-controlled SCLC. The total different conduction behavior in ON and OFF states suggests that the high conductivity in ON state cells should be a confined, filamentary effect rather than a homogenously distributed one.[9]

Ag, as we know, is easy to be ionized, and Ag ions are apt to diffusing and forming Ag filaments as applying a positive voltage bias on Ag electrodes. Therefore, the RS of the ITO/6F-BAHP-PC PI/Ag devices may originate from the forming/rupture of Ag filaments in the 6F-BAHP-PC PI. To ascertain whether the observed RS behavior of the 6F-BAHP-PC PI device is from the polymer layer itself or Ag filaments, a negative bias was applied to the device, namely, the positive bias was applied to ITO electrodes. The devices are found to switch from OFF to ON state at about −1.37 V and from ON to OFF state at about −0.6 V with an ON/OFF ratio of more than 10^6, as shown in Fig. 8(a). Furthermore, using an inert metal (Pt) as top electrodes, a similar RS phenomenon has also been observed, as shown in Fig. 8(b). Therefore, it can be confirmed that for the ITO/6F-HAB-DPC PI/Pt devices, the RS is from the polymer layer itself rather than Ag filaments.

In the 6F-BAHP-PC PI chain, pendant 9-phenyl-9*H*-carbazole moieties are electron donors and act as nucleophilic sites, whereas trifluoromethyl groups and imide rings are electron acceptors and act as electrophilic sites. These two parts are linked through a nonconjugational chain, so the intramolecular charge transfer is minimized. Fig. 9 shows the energy level diagram of

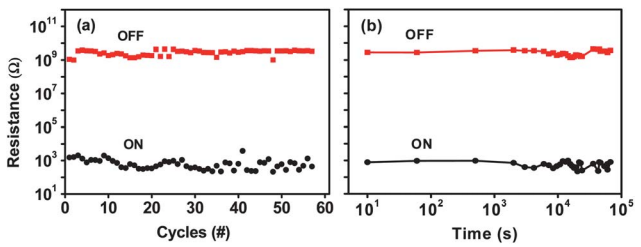

Fig. 6 (a) The endurance performance and (b) retention for the ON and OFF states of the ITO/6F-BAHP-PC PI/Ag memory cells.

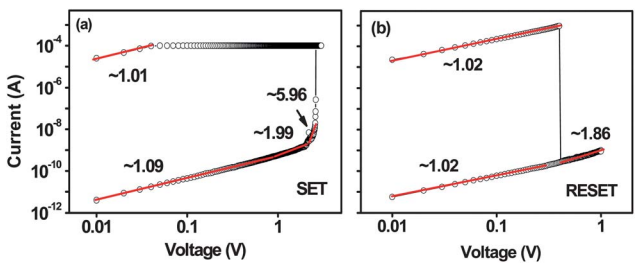

Fig. 7 *I–V* curves of the ITO/6F-BAHP-PC PI/Ag memory cells plotted on a log-log scale and the linear fitting results in both ON and OFF states in the processes of (a) SET and (b) RESET. Also shown are the corresponding slopes for different portions.

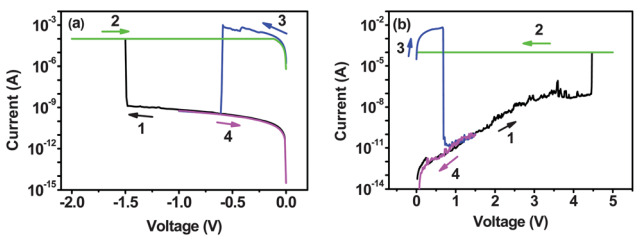

Fig. 8 *I–V* characteristics of (a) ITO/6F-BAHP-PC PI/Ag memory cells where a negative bias was applied to the devices and (b) ITO/6F-BAHP-PC PI/Pt memory cells where a positive bias was applied to the devices.

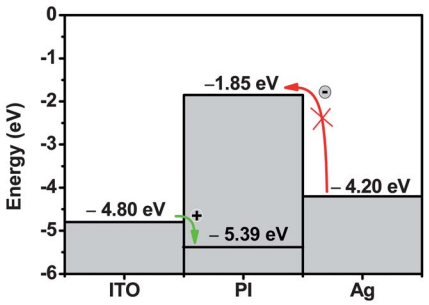

Fig. 9 Energy level diagram of ITO/6F-BAHP-PC PI/Ag device.

ITO/6F-BAHP-PC PI/Ag devices. The energy barrier for hole injection from the bottom electrode to the active PI layer was estimated to be 0.94 eV according to the work function of ITO and HOMO level of the active PI layer. The energy barrier for electron injection from the top electrode to the active layer was estimated to be 2 eV according to the work function of Ag and LUMO level of the active PI layer. Thus, for the 6F-BAHP-PC PI, the energy barrier for hole injection from ITO electrode is much lower than that for electron injection from Ag electrode. Therefore, the conduction process in the device is likely to be dominated by hole injection. With an increase in voltage, holes are injected from the ITO into the polymer gradually. These charges can move by a hopping process through the polymer chain. Charge trapping sites in the polymer can lead to charge accumulation and then redistribution of the electric field. At the threshold voltage under a current compliance of 0.1 mA, nearly all pendant 9-phenyl-9*H*-carbazole moieties are filled with holes, and then the charges will have high mobility, namely, conducting filaments form. The charges can flow through the filaments and sustain the ON state. When the current compliance increases to 1 mA, a large number of charges flow through the previously formed filaments, and this process might produce an excess of heat. In addition, along with the increase of current through the filaments, the number of charges injected into the polyimide film is also increased and the charges can be trapped in the PI layer and the interface between the PI and electrode. When the voltage bias exceeds a certain value, the number of injected charges will rise more than the capacity of the filaments. Such excessive current flow will also generate additional heat. Meanwhile, the excessive current flow may lead to repulsive coulombic interactions between the trapped charges gathering in the polyimide layer and in the interface. The generated heat and repulsive coulombic interactions will cause rupture of the filaments formed in the switch-ON process. As a result, the device is switched back to its initial OFF state.

To provide direct experimental evidence of the filamentary mechanism of the RS in 6F-BAHP-PC PI, *in situ* C-AFM measurements have been performed. During the measurements, the Pt/Ir coated conductive tip was grounded and directly touched the 6F-BAHP-PC PI films. The schematic measurement configuration is shown in Fig. 10(a). The voltage was applied to the bottom electrode (ITO). C-AFM measurements were performed in the same region of 2 × 2 μm^2 in size under various external voltage biases. The initial resistance of the films is very high, no obvious leakage can be observed under a voltage of 0–6 V (Fig. 10(b)). Therefore, the pristine 6F-BAHP-PC PI is in the OFF state. As shown in Fig. 10(c), when applying an 8 V bias, several highly conductive spots can be observed in the C-AFM current map, with diameters of about 30–50 nm. It indicates that the films undergo electrical transition from the OFF state to the ON state. The number and current height of the conductive pots increase with the voltage, as shown in Fig. 10(d). The C-AFM results confirm that the RS of 6F-BAHP-PC PI originates from the formation/rupture of conducting filaments.

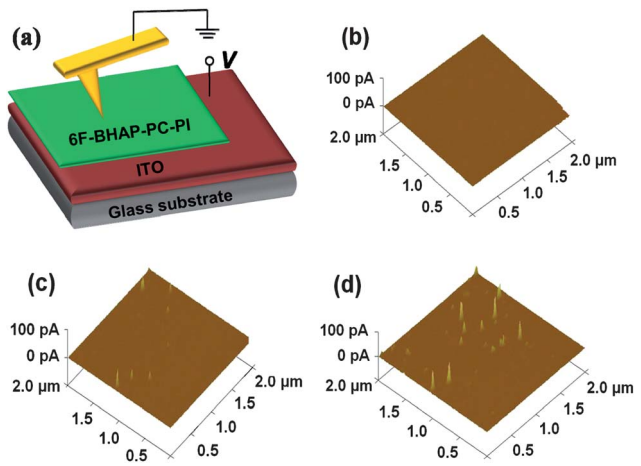

Fig. 10 C-AFM measurements on a 6F-BAHP-PC PI film. (a) Schematic measurement configuration, (b) $V = 6$ V, (c) $V = 8$ V, and (d) $V = 10$ V.

Conclusions

In this study, we have successfully synthesized a novel polyimide (6F-BAHP-PC PI) functionalized by a stable hole-transporting and donor unit bearing 9-phenyl-9*H*-carbazole pendant. This polyimide exhibits good solubility in common organic solvents and good thermal stability. The optical band gap of 6F-BAHP-PC PI is 3.54 eV and the onset oxidation potential is 1.26 V, indicating that such polyimide could provide a lower and more stable HOMO energy. The ITO/6F-BAHP-PC PI/Ag memory devices show nonvolatile unipolar RS with an ON/OFF ratio of 10^6, power consumption of ~100 μW, good endurance and retention performance. The dominant conduction mechanisms in the ON and OFF states are ohmic behavior and trap-controlled SCLC, respectively. The RS of ITO/6F-BAHP-PC PI/Ag devices is attributed to the formation/rupture of nanoscale conducting filaments. The high ON/OFF ratio, good endurance and retention, and low power consumption of ITO/6F-BAHP-PC PI/Ag devices open the door to the possibility of mass production of high performance nonvolatile memory devices at low cost.

Acknowledgements

The authors acknowledge financial support from the Chinese Academy of Sciences (CAS), State Key Project of Fundamental Research of China (973 Program), the National Natural Science Foundation of China, Zhejiang Qianjiang Talent Project, Zhejiang and Ningbo Natural Science Foundations.

References

1 T. W. Hickmott, *J. Appl. Phys.*, 1962, **33**, 2669–2682.
2 K. Terabe, T. Hasegawa, T. Nakayama and M. Aono, *Nature*, 2005, **433**, 47–50.
3 R. Waser, R. Dittmann, G. Staikov and K. Szot, *Adv. Mater.*, 2009, **21**, 2632–2663.
4 Z. Yan, Y. Guo, G. Zhang and J. M. Liu, *Adv. Mater.*, 2011, **23**, 1351–1355.
5 M. Li, F. Zhuge, X. J. Zhu, K. Yin, J. Wang, Y. W. Liu, C. L. He, B. Chen and R. W. Li, *Nanotechnology*, 2010, **21**, 425202.
6 S. H. Jo, T. Chang, I. Ebong, B. B. Bhadviya, P. Mazumder and W. Lu, *Nano Lett.*, 2010, **10**, 1297–1301.
7 J. Yao, Z. Sun, L. Zhong, D. Natelson and J. M. Tour, *Nano Lett.*, 2010, **10**, 4105–4110.
8 J. J. Yang, M. D. Pickett, X. Li, A. A. OhlbergDouglas, D. R. Stewart and R. S. Williams, *Nat. Nanotechnol.*, 2008, **3**, 429–433.

9 F. Zhuge, W. Dai, C. L. He, A. Y. Wang, Y. W. Liu, M. Li, Y. H. Wu, P. Cui and R. W. Li, *Appl. Phys. Lett.*, 2010, **96**, 163505.
10 Q.-D. Ling, Y. Song, S.-L. Lim, E. Y.-H. Teo, Y.-P. Tan, C. Zhu, D. S. H. Chan, D.-L. Kwong, E.-T. Kang and K.-G. Neoh, *Angew. Chem., Int. Ed.*, 2006, **45**, 2947–2951.
11 S. Baek, D. Lee, J. Kim, S.-H. Hong, O. Kim and M. Ree, *Adv. Funct. Mater.*, 2007, **17**, 2637–2644.
12 Q.-D. Ling, E.-T. Kang, K.-G. Neoh, Y. Chen, X.-D. Zhuang, C. Zhu and D. S. H. Chan, *Appl. Phys. Lett.*, 2008, **92**, 143302.
13 T.-W. Kim, H. Choi, S.-H. Oh, G. Wang, D.-Y. Kim, H. Hwang and T. Lee, *Adv. Mater.*, 2009, **21**, 2497–2500.
14 T. J. Lee, S. Park, S. G. Hahm, D. M. Kim, K. Kim, J. Kim, W. Kwon, Y. Kim, T. Chang and M. Ree, *J. Phys. Chem. C*, 2009, **113**, 3855–3861.
15 X.-D. Zhuang, Y. Chen, B.-X. Li, D.-G. Ma, B. Zhang and Y. Li, *Chem. Mater.*, 2010, **22**, 4455–4461.
16 Q.-D. Ling, F.-C. Chang, Y. Song, C.-X. Zhu, D.-J. Liaw, D. S.-H. Chan, E.-T. Kang and K.-G. Neoh, *J. Am. Chem. Soc.*, 2006, **128**, 8732–8733.
17 S. G. Hahm, S. Choi, S.-H. Hong, T. J. Lee, S. Park, D. M. Kim, W.-S. Kwon, K. Kim, O. Kim and M. Ree, *Adv. Funct. Mater.*, 2008, **18**, 3276–3282.
18 S. G. Hahm, S. Choi, S.-H. Hong, T. J. Lee, S. Park, D. M. Kim, J. C. Kim, W. Kwon, K. Kim, M.-J. Kim, O. Kim and M. Ree, *J. Mater. Chem.*, 2009, **19**, 2207–2214.
19 D. M. Kim, S. Park, T. J. Lee, S. G. Hahm, K. Kim, J. C. Kim, W. Kwon and M. Ree, *Langmuir*, 2009, **25**, 11713–11719.
20 K. Kim, S. Park, S. G. Hahm, T. J. Lee, D. M. Kim, J. C. Kim, W. Kwon, Y.-G. Ko and M. Ree, *J. Phys. Chem. B*, 2009, **113**, 9143–9150.
21 T. J. Lee, C. W. Chang, S. G. Hahm, S. Park, D. M. Kim, J. Kim, W.-S. Kwon, G.-S. Liu and M. Ree, *Nanotechnology*, 2009, **20**, 135204.
22 Y. L. Liu, Q. D. Ling, E. T. Kang, K. G. Neoh, D. J. Liaw, K. L. Wang, W. T. Liou, C. X. Zhu and D. S. H. Chan, *J. Appl. Phys.*, 2009, **105**, 044501.
23 Y.-L. Liu, K.-L. Wang, G.-S. Huang, C.-X. Zhu, E.-S. Tok, K.-G. Neoh and E.-T. Kang, *Chem. Mater.*, 2009, **21**, 3391–3399.
24 N.-H. You, C.-C. Chueh, C.-L. Liu, M. Ueda and W.-C. Chen, *Macromolecules*, 2009, **42**, 4456–4463.
25 T. Kuorosawa, C.-C. Chueh, C.-L. Liu, T. Higashihara, M. Ueda and W.-C. Chen, *Macromolecules*, 2010, **43**, 1236–1244.
26 Q. Liu, K. Jiang, L. Wang, Y. Wen, J. Wang, Y. Ma and Y. Song, *Appl. Phys. Lett.*, 2010, **96**, 213305.
27 K.-L. Wang, Y.-L. Liu, J.-W. Lee, K.-G. Neoh and E.-T. Kang, *Macromolecules*, 2010, **43**, 7159–7164.
28 K.-L. Wang, Y.-L. Liu, I. H. Shih, K.-G. Neoh and E.-T. Kang, *J. Polym. Sci., Part A: Polym. Chem.*, 2010, **48**, 5790–5800.
29 Y.-S. Lai, C.-H. Tu, D.-L. Kwong and J. S. Chen, *Appl. Phys. Lett.*, 2005, **87**, 122101.
30 Q.-D. Ling, S.-L. Lim, Y. Song, C.-X. Zhu, D. S.-H. Chan, E.-T. Kang and K.-G. Neoh, *Langmuir*, 2007, **23**, 312–319.
31 S. L. Lim, N.-J. Li, J.-M. Lu, Q.-D. Ling, C. X. Zhu, E.-T. Kang and K. G. Neoh, *ACS Appl. Mater. Interfaces*, 2009, **1**, 60–71.
32 C.-L. Liu, J.-C. Hsu, W.-C. Chen, K. Sugiyama and A. Hirao, *ACS Appl. Mater. Interfaces*, 2009, **1**, 1974–1979.
33 J. Ouyang, C.-W. Chu, C. R. Szmanda, L. Ma and Y. Yang, *Nat. Mater.*, 2004, **3**, 918–922.
34 R. J. Tseng, J. Huang, J. Ouyang, R. B. Kaner and Y. Yang, *Nano Lett.*, 2005, **5**, 1077–1080.
35 Q. X. Lai, Z. Y. Li, L. Zhang, X. M. Li, W. F. Stickle, Z. H. Zhu, Z. Gu, T. I. Kamins, R. S. Williams and Y. Chen, *Nano Lett.*, 2008, **8**, 876–880.
36 J. Y. Ouyang and Y. Yang, *Appl. Phys. Lett.*, 2010, **96**, 063506.
37 B. Mukherjee, S. K. Batabyal and A. J. Pal, *Adv. Mater.*, 2007, **19**, 717–722.
38 G. Liu, Q.-D. Ling, E. Y. H. Teo, C.-X. Zhu, D. S.-H. Chan, K.-G. Neoh and E.-T. Kang, *ACS Nano*, 2009, **3**, 1929–1937.
39 J. Yao, Z. Jin, L. Zhong, D. Natelson and J. M. Tour, *ACS Nano*, 2009, **3**, 4122–4126.
40 G. Liu, X. Zhuang, Y. Chen, B. Zhang, J. Zhu, C.-X. Zhu, K.-G. Neoh and E.-T. Kang, *Appl. Phys. Lett.*, 2009, **95**, 253301.
41 G. L. Li, G. Liu, M. Li, D. Wan, K. G. Neoh and E. T. Kang, *J. Phys. Chem. C*, 2010, **114**, 12742–12748.
42 X.-D. Zhuang, Y. Chen, G. Liu, P.-P. Li, C.-X. Zhu, E.-T. Kang, K.-G. Noeh, B. Zhang, J.-H. Zhu and Y.-X. Li, *Adv. Mater.*, 2010, **22**, 1731–1735.
43 Z. J. Donhauser, B. A. Mantooth, K. F. Kelly, L. A. Bumm, J. D. Monnell, J. J. Stapleton, D. W. Price, Jr., A. M. Rawlett, D. L. Allara, J. M. Tour and P. S. Weiss, *Science*, 2001, **292**, 2303–2307.
44 Q. Ling, Y. Song, S. J. Ding, C. Zhu, D. S. H. Chan, D.-L. Kwong, E.-T. Kang and K.-G. Neoh, *Adv. Mater.*, 2005, **17**, 455–459.
45 J. Smits, S. J. Meskers, R. Janssen, A. Marsman and D. de Leeuw, *Adv. Mater.*, 2005, **17**, 1169–1173.
46 Y. Yang, J. Ouyang, L. Ma, R. J.-H. Tseng and C.-W. Chu, *Adv. Funct. Mater.*, 2006, **16**, 1001–1014.
47 J.-F. Morin and M. Leclerc, *Macromolecules*, 2002, **35**, 8413–8417.
48 Z.-K. Xu, B.-K. Zhu and Y.-Y. Xu, *Chem. Mater.*, 1998, **10**, 1350–1354.
49 H. Xin, F. Y. Li, M. Guan, C. H. Huang, M. Sun, K. Z. Wang, Y. A. Zhang and L. P. Jin, *J. Appl. Phys.*, 2003, **94**, 4729–4731.
50 F. Sanda, T. Nakai, N. Kobayashi and T. Masuda, *Macromolecules*, 2004, **37**, 2703–2708.
51 X. D. Zhuang, Y. Chen, G. Liu, B. Zhang, K. G. Neoh, E. T. Kang, C. X. Zhu, Y. X. Li and L. J. Niu, *Adv. Funct. Mater.*, 2010, **20**, 2916–2922.
52 Y.-K. Fang, C.-L. Liu and W.-C. Chen, *J. Mater. Chem.*, 2011, **21**, 4778–4786.
53 Y. Zhang, L. Wang, T. Wada and H. Sasabe, *Appl. Phys. Lett.*, 1997, **70**, 2949–2951.
54 G. L. Tullos, J. M. Powers, S. J. Jeskey and L. J. Mathias, *Macromolecules*, 1999, **32**, 3598–3612.
55 Q.-D. Ling, D.-J. Liaw, C. Zhu, D. S.-H. Chan, E.-T. Kang and K.-G. Neoh, *Prog. Polym. Sci.*, 2008, **33**, 917–978.

